Journal of Ovonic Research Vol. 14, No. 4, July - August 2018, p. 293 - 305

THE INFLUENCE OF DEPOSITION TIME AND ANNEALING TEMPERATURE ON THE OPTICAL PROPERTIES OF CHEMICALLY DEPOSITED CERIUM OXIDE (CeO) THIN FILM

P. N. KALU[a,b*], D. U. ONAH[b], P. E. AGBO[b], C. AUGUSTINE[a], R. A. CHIKWENZE[a], F. N. C. ANYAEGBUNAM[a] , C. O. DIKE[a]
[a]*Department of Physics/Geology/Geophysics, Alex Ekwueme Federal University Ndufu-Alike Ikwo, Nigeria*
[b]*Department of Industrial Physics, Ebonyi State University, Abakaliki, Nigeria*

The chemical bath deposition technique was applicable in the deposition of CeO thin films on glass substrates directly from aqueous solutions containing cerium acetate precursors. UV-Vis spectrophotometry measurements give a transparency of around 65-75% in the visible range (400-700 nm) for the films with different growth parameters. The absorbance increased with deposition time exhibiting a maximum in the UV region. Direct band gap energy of these samples were measured to be in the range of 3.5-3.90 eV for as-deposited, 3.45-3.85eV for annealed at 100^{o}C, 3.80-3.85eV for annealed at 150^{o}C and 3.65-3.75eV for annealed at 200^{o}C at different deposition time while indirect band gap values of 3.00-3.50eV, 3.20-3.60eV, 3.25-3.65eV and 2.80-3.50eV were recorded for as-deposited, annealed at 100^{o}C, 150^{o}C and 200^{o}C respectively at different deposition time. The band gap values both direct and indirect indicated a considerable variation with growth parameters. Furthermore, a red shift was observed with increasing annealing temperature for the films at 1 and 3 hours deposition time, which resulted in a decrease in the optical direct band gap whereas a blue shift was observed for the films at 2 hours deposition time at different annealing temperatures. The Urbach energy values were found to vary in the range of 3.00-3.50eV for as-deposited to 3.25-3.60eV for annealed at 100^{o}C to 3.25-3.35eV for annealed at 150^o to 2.80-3.50eV for annealed at 200^{o}C at different deposition time. The Urbach energy exhibited increasing trend with annealing temperature except for the films deposited at 3hours which depicts a reversed trend. The Urbach energy also increases with deposition time for some of the film samples. Based on the exhibited properties of the film, it can be concluded that it is a promising material for selective coatings for solar cells, effective coatings for poultry houses, use as antireflective coating materials and for fabrication of optoelectronic devices.

(Received March 27, 2018; Accepted August 10, 2018)

Keywords: Band gap, Temperature, Thin film, Urbach energy, Transmittance

1. Introduction

In recent times, metal oxide semiconductors have attracted the attention of solid state researchers due to their verse applications in medicine, industries etc. Other notable applications of metal oxides are in photodiodes, phototransistors, photovoltaics, transparent electrodes, liquid crystal displays, IR detectors and anti-reflection coating [1]. There are many publications focussing on different types of these materials namely, NiO, Mn_3O_4, CuO, TiO_2, ZnO, Cr_3O_4, Fe_3O_4 and CeO. The growing interest in the use of CeO is due to its properties such as wide band gap of about 3.2eV [2, 3], transparent in the visible region (400-800nm) [2, 3], and can be prepared using relatively cheap deposition technique. These properties placed CeO as suitable materials for use in applications such as electrochemical displays [4], smart windows [5], oxygen storage [6], catalysts [7] and UV filters [8].

The survey of literature shows that CeO have been prepared by several deposition methods, including spin coating [9, 10], pulsed laser deposition [11], spray pyrolysis [12], sputtering [13] and chemical bath deposition [14]. The chemical deposition route is gaining recognition as it is

relatively inexpensive, simple and convenient for large area deposition. It does not require sophisticated instrumentation like vacuum systems and other expensive equipment. The starting chemicals are cheap and commonly available. With chemical deposition, a large number of substrates can be coated in a single run with a proper jig design. Unlike in ED, electrical conductivity of the substrate is not a necessary requirement in chemical deposition [15]. Hence, any insoluble surface to which the solution has free access will be a suitable substrate for deposition [15]. The low temperature deposition avoids oxidation or corrosion of metallic substrates. The preparative parameters are easily controllable and better orientation and improved grain structure can be obtained [15].

The objective of this research was to prepare CeO thin films on commercially purchased microscopic glass substrates using chemical bath deposition and to study the effects of deposition time and annealing temperatures on the optical properties of the films.

2. Experimental

CeO thin films have been synthesized by chemical bath deposition technique from a mixture of 15ml of 0.2M $Ce(NO_3)_2$, 15ml of 0.2M of sodium thiosulphate with 2 drops of NH_3 (ammonia). Sodium thiosulphate acted as complexing agent to facilitate the precipitation of the cations and anions which combined to form a neutral compound. The bath was allowed to stand for 1, 2 and 3 hours deposition time at a temperature of 70^0C.The microscopic glass slides used as substrates prior to deposition were soaked in concentrated hydrochloric acid for 24 hours, removed and washed with foam-sponge in ethanol and finally rinsed in distilled water. Thereafter, they were then drip dried in air. The degreased, cleaned surface has the advantage of providing nucleation centers for the growth of the films, hence, yielding highly adhesive and uniformly deposited films. Thermo scientific GENESYS 10S model UV-VIS spectrophotometer was used to determine the transmittance of the deposited films in the wavelength range of 300-1000 nm. The kinetics of the chemical reaction proceeded as follows:

$$Ce(NO_3)_2 \rightarrow Ce^{2+} + NO_3{}^{2-}$$
$$NH_3.H_2O \rightarrow NH_4{}^{+} + OH^{-}$$
$$Ce^{2+} + OH^{-} \rightarrow Ce(OH)_2$$
$$Ce(OH)_2 \rightarrow CeO + H_2O$$

3. Results and discussion

Fig.1 gives absorbance versus wavelength spectra for the films deposited at 1 hour deposition time at different annealing temperatures. Fig.2 depicts the plots of absorbance versus wavelength spectra of the films deposited at 2 hours at different annealing temperature while the plots of absorbance versus wavelength spectra for the films deposited at 3 hours at different annealing temperatures is shown in Fig.3. From Fig.1, the absorbance vary from 0.3 to 1.63, 0.25 to 0.80, 0.125 to 2.20 and 0.65 to 1.63 for as-deposited, annealed at 100^{o}C, 150^{o}C and 200^{o}C respectively. When deposition time was increased to 2 hours, the absorbance vary from 1.0-2.30 for as-deposited sample, 1.10-2.70 for sample annealed at 100^{o}C, 0.1-1.15 for sample annealed at 150^{o}C and 0.20-0.95 for sample annealed at 200^{o}C. As observed in Fig.3, the absorbance of the films deposited at 3 hours deposition time vary in a similar manner, decreasing from 2.65 to 0.35, 2.45 to 0.50, 1.13 to 0.25 and 1.20 to 0.25 for as-deposited, annealed at 100^{o}C, 150^{o}C and 200^{o}C respectively. A close look at the figures indicate an increase in absorbance with deposition time exhibiting a maximum for the films deposited at 3 hours deposition time. With respect to annealing temperature, the absorbance of the films depict lack of trend for the films deposited at 1 and 2 hours deposition time. The absorbance shows strong correlation with annealing temperature for the films deposited at 3 hours deposition time. In all deposition parameters, the absorbance

generally decreased with wavelength remaining fairly constant within 400-1000nm wavelength range. The maximum absorbance for the films is about 3.00 (arb. Unit) which is higher than 2.0 (arb unit) stipulated by lambert-Beer's law. This could be attributed to the concentration of the reagents used. At high concentrations, the assumptions of Lambert-Beer law no longer hold [16]. Particle attractive forces come into play at high concentrations, resulting to the tendency of the particles to absorb more light. Thus, most of the light is absorbed by the particles thereby reducing the transmission of light as it passes through the sample. The high absorbance of the films suggest that they could be used as spectral selective coating on collectors for enhanced solar energy collection. This way, enormous heat could be generated to produce boiler for thermal power plants to generate electricity. Figures 4, 5 and 6 shows the transmittance spectra for the films deposited at 1, 2 and 3 hours deposition time at different annealing temperature respectively. The transmittance varied considerably with annealing temperatures exhibiting a maximum of 75% for the films annealed at 150^{o}C. For the films deposited at 1 hour deposition time at different annealing temperatures, the transmittance exhibit a maximum of 65%, 60%, 75% and 35% for as-deposited, annealed at 100^{o}C, 150^{o}C and 200^{o}C film samples respectively. In the case of the films deposited at 2 hours deposition time, the maximum transmittances are 10%, 7.5%, 75% and 62.5% for as-deposited, annealed at 100^{o}C, 150^{o}C and 200^{o}C respectively. When deposition time was increased to 3 hours, the maximum transmittance vary from 40% for as-deposited sample to 35% for annealed at 100^{o}C to 64% for annealed at 150^{o}C to 55% for annealed at 200^{o}C. A steep fall in the fundamental edge independent of the post-deposition heat treatments was observed for the films. This observation has been attributed to better crystal ordering due to the post-deposition heat treatments. The transmittance of thin films can be greatly modified by different deposition variables. The annealing temperature optical dependent behaviour has been reported by other authors in the following reference in the literature [17-21]. The variation of concentration and deposition time on the transmittance of thin films have been reported [22-25].

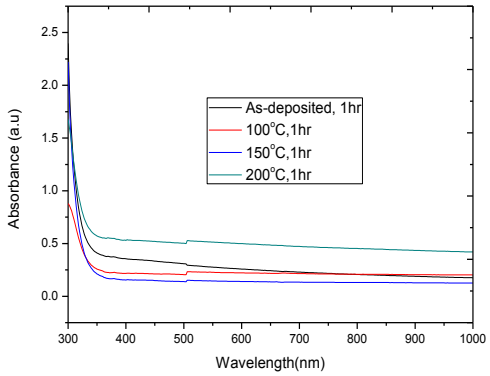

Fig.1. Plots of absorbance versus wavelength for films deposited at 1hour at different annealing temperatures.

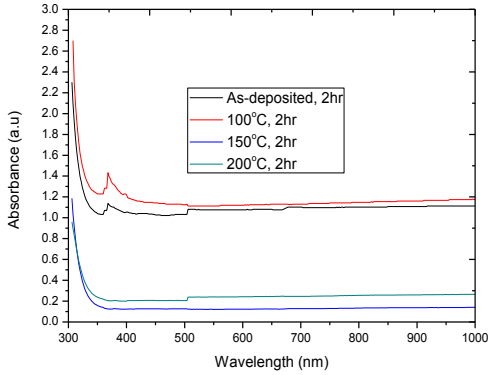

Fig. 2. Plots of absorbance versus wavelength for films deposited at 2 hours at different annealing temperatures

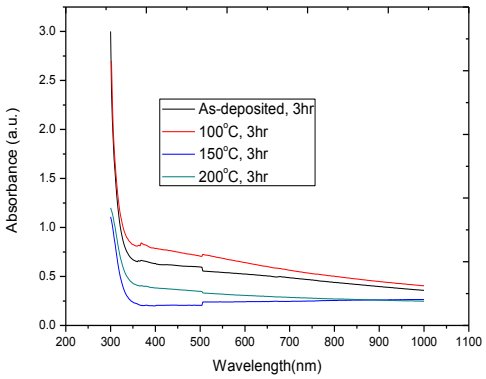

Fig. 3. Plots of absorbance versus wavelength for films deposited at 2 hours at different annealing temperature.

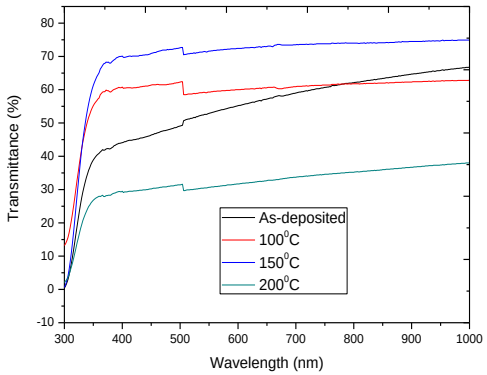

Fig. 4. Transmittance spectra for films deposited at 1 hour at different annealing temperature.

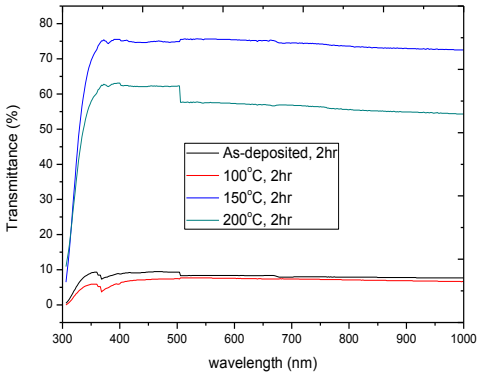

Fig. 5. Transmittance spectra for films deposited at 2 hours at different annealing temperature.

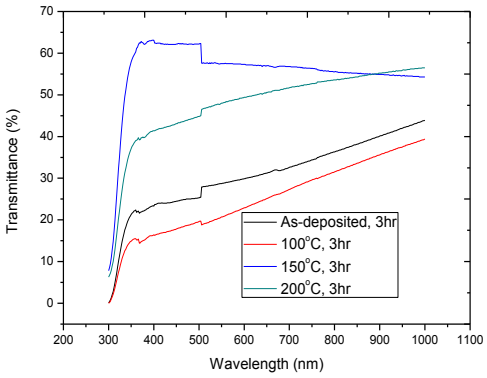

Fig. 6. Transmittance spectra for films deposited at 3 hours at different annealing temperature.

Direct energy gap was determined by plotting a graph of $(\alpha h\nu)^2$ versus $h\nu$ and extrapolation of straight line to $(\alpha h\nu)^2 = 0$ gives the direct band gap values at different deposition time and annealing temperatures (Figs. 7-9) while Fig. 9-12 depicts the plots of $(\alpha h\nu)^{1/2}$ versus hv for the estimation of the indirect band gap. The values of the direct band gap at different deposition time and annealing temperature are tabulated in Table 1 while that of indirect band gap is shown in Table 2. The tables are extracts from Figures 7-12. Studies of table 1 shows that the direct band gap vary in the range 3.35-4.00eV for films deposited at 1 hour deposition time at different annealing temperature, 3.78-3.85eV for films deposited at 2 hours deposition time at different annealing temperature and 3.25-3.90eV for films deposited at 3 hours deposition time at different annealing temperature. Generally, there is lack of trend with annealing temperature with respect to the band gaps. However, some of the film samples exhibited some form of correlation with increase in annealing temperature. With respect to deposition time, a clear trend was observed for most of the film samples. In particular, the band gap increases with deposition time for the film samples annealed at 100^o for both direct and indirect while it decreases for the annealed at 150^oC. It is noticed that the indirect band gap increased with deposition time from 3.40eV to 3.80eV for the film annealed at 100^oC, decreases from 3.65eV to 3.50eV for films annealed at 150^oC and has no trend with deposition time for the films annealed at 200^oC. A clear variation of the band gap of the films with growth parameters indicates that we can tune the solid state properties of films to suite a desired application. The changes in band gap as value of parameter of growth changes is not unconnected with the size distribution of the crystallites of the films. In view of the required band gap energy for the various layers of heterojunction solar cells, the CeO films deposited at various conditions can be said to exhibit high values of band gap, as observed in the tables and also transparent in the visible region, which is the spectral region of importance for photovoltaic application. The primary function of a window layer in a heterojunction is to form a junction with the absorber layer while admitting a maximum amount of light to the junction region and the absorber layer. For high optical output with minimal resistive loss the band gap of the window layer should be as high as possible and as thin as possible to maintain a low series resistance [26]. The CIGS solar cells typically use a CdS window layer, which is deposited by CBD technique, and which is believed to provide superior performance compared with that deposited by a physical vapour deposition technique [26]. However, there are great concern about the toxicity of Cd in this architecture [27] and so; several alternative window layers are currently being investigated to replace CdS. CeO thin films deposited in this work stand high for possible incorporation in CIGS solar cell and has also the potential to improve the blue response in the device.

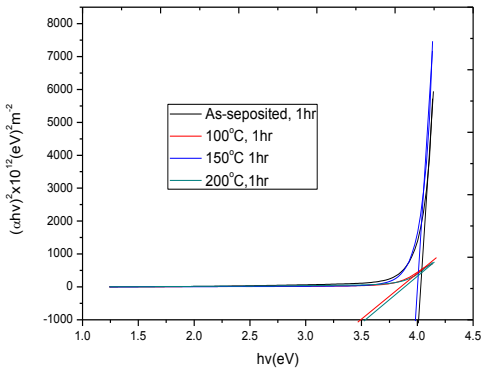

Fig. 7. Plots of $(\alpha hv)^2$ versus hv for samples deposited at 1 hour at different annealing temperature

Table 1. Direct band gap values of film samples deposited at different deposition time and annealing temperature .

Deposition time (hours)	E_g (eV) before annealing	E_g (eV) after annealing at		
		100°C	150°C	200°C
1	3.90	3.35	4.00	3.50
2	3.78	3.80	3.85	3.75
3	3.90	3.85	3.30	3.25

Table 2. Indirect band gap values of film samples deposited at different deposition time and annealing temperature.

Sample	E_g (eV) before annealing	E_g (eV) after annealing at		
		100°C	150°C	200°C
1	3.75	3.40	3.65	3.50
2	3.40	3.50	3.60	3.45
3	3.65	3.80	3.50	3.20

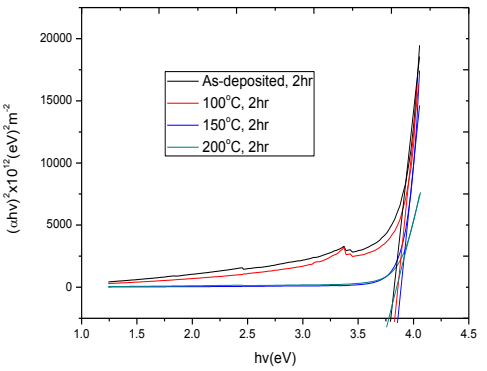

Fig. 8. Plots of $(\alpha hv)^2$ versus hv for samples deposited at 2 hours at different annealing temperature.

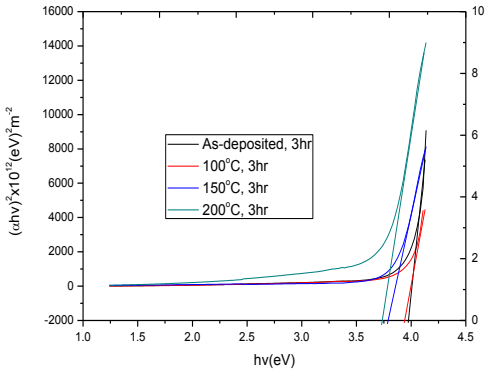

Fig.9. Plots of $(\alpha hv)^2$ versus hv for samples deposited at 3 hours at different annealing temperature.

The range of indirect band gap values for the films are in good agreement with the report of other research group [10]. The band gaps were calculated using already established equation [28].

$$(\alpha hv)^n = A(hv - E_g) \tag{1}$$

where A is band edge parameter and value of n determines the nature of optical transition (n = ½ indicates direct transition and n = 2 indicates indirect transition).

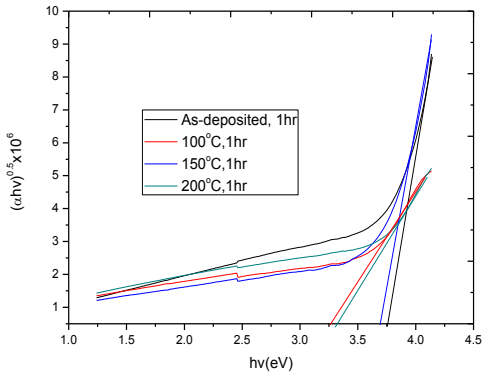

Fig.10. Plots of $(\alpha hv)^{1/2}$ versus hv for samples deposited at 1 hour at different annealing temperature.

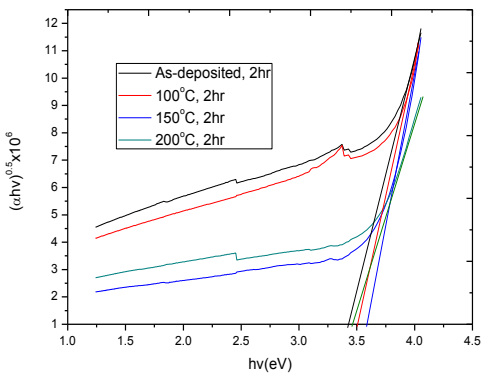

Fig.11. Plots of $(\alpha hv)^{1/2}$ versus hv for samples deposited at 2 hours at different annealing temperature.

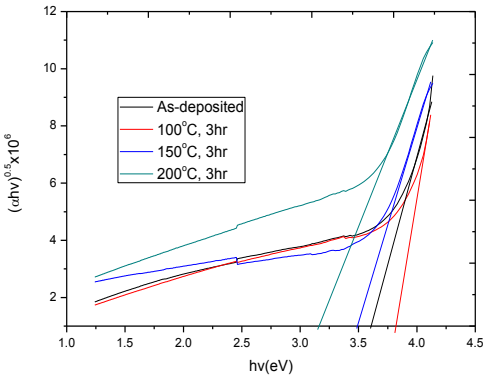

Fig. 12. Plots of $(\alpha hv)^{1/2}$ versus hv for samples deposited at 3 hours at different annealing temperature.

The Urbach energy tails define the amount of defects present in thin films. These energy tails have correlation with the width of the localized states available in the optical band gap of the thin films. This width, of the localized states, is related directly to a similar exponential tail for the density of states near band edges and can be expressed by the temperature and spectral dependence of absorption coefficient [29, 30].

$$\alpha = \alpha_o \exp\left(\frac{h\nu}{E_u}\right) \tag{2}$$

where α_o is a constant, E_u denotes an energy which is constant or weakly dependent on temperature and is often interpreted as the width of the tail of localized states in the band gap. The exponential tail appears because disordered and amorphous materials produce localized states extended in the band gap [31]. The band tail energy or Urbach energy (E_u) can be obtained from the slope of the straight line of plotting $\ln(\alpha)$ against the incident photon energy ($h\nu$). Figure 13 to 15 illustrates the plots of ln α versus photon energy ($h\nu$) for the films at different deposition time and annealing temperatures. Eu values were calculated from reciprocal of the straight line slopes, as shown in the Figure 13-15, and presented in Table 3. Generally, the Urbach energy exhibited a blue shift for the annealed layers except for the film samples deposited at 3 hours which shows lack of trend. Such increase in Urbach energy with increasing annealing temperature have been reported by other research groups for different thin film materials [32].

Table 3. Urbach energy tail values of film samples at different deposition time and annealing temperature .

Deposition time (hours)	E_g (eV) before annealing	E_g (eV) after annealing at		
		100°C	150°C	200°C
1	3.60	3.30	3.50	3.35
2	3.20	3.35	3.50	3.45
3	3.50	3.65	3.25	2.90

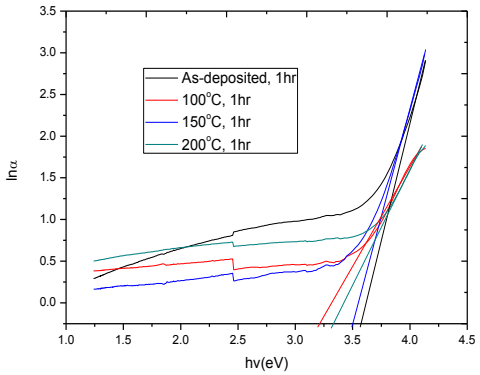

Fig. 13. Plots of $\ln(\alpha)$ *versus hv of film samples deposited at 1 hour at different annealing temperature.*

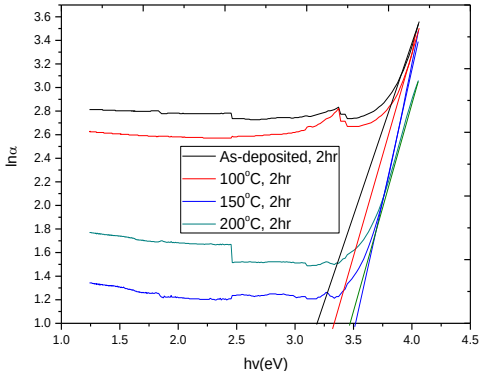

Fig. 14. Plots of $\ln(\alpha)$ *versus hv of film samples deposited at 2 hours at different annealing temperature.*

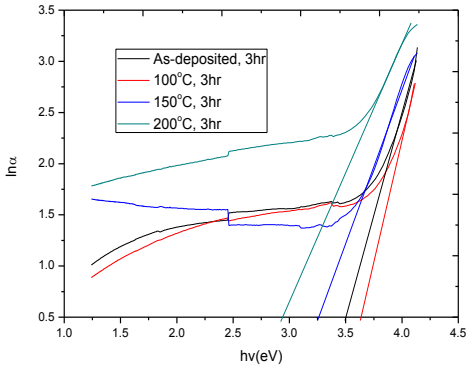

Fig. 15. Plots of $\ln(\alpha)$ *versus hv of film samples deposited at 3 hours at different annealing temperature.*

The variation of extinction coefficient against photon energy (hν) at different deposition time and annealing temperatures are indicated in Fig.16, 17 and 18 respectively. It is observed that the plots of extinction coefficient indicates a lack of trend with respect to deposition parameters. Generally, the heated layers have higher extinction coefficient values compared to the as-deposited layers. Fig.16 shows that the film annealed at 150°C has a maximum value ≤ 16.5 while the annealed at 100°C has a maximum value ≤ 95 (Fig.17) and annealed at 200°C has a maximum value ≤ 37 (Fig.18). The extinction coefficient was fairly constant between 1.25eV to

3.50eV for the film samples except for few exceptions. A steady rise was observed at 3.75eV up to 4.00eV. The extinction coefficient, k was calculated using the relation [33]. Where all symbols retain their usual meaning.

$$k = \frac{\alpha\lambda}{4\pi} \tag{3}$$

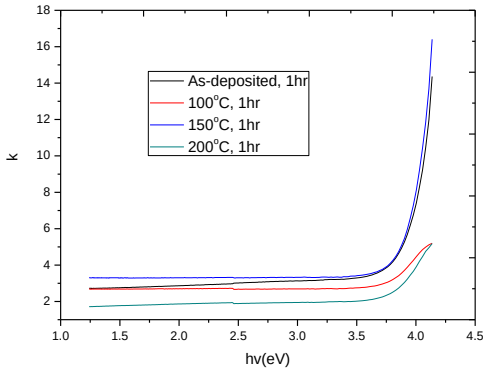

Fig. 16. Plots of k versus hv of film samples at 1 hour deposition time at different annealing temperature.

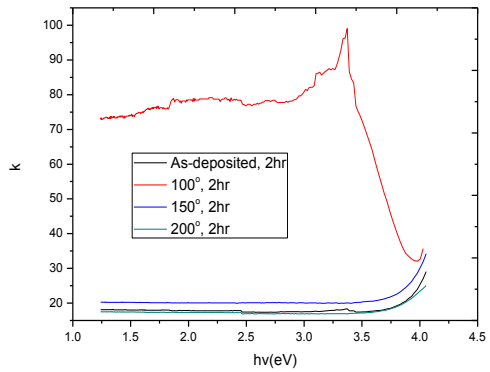

Fig. 17. Plots of k versus hv of film samples at 2 hours deposition time at different annealing temperature.

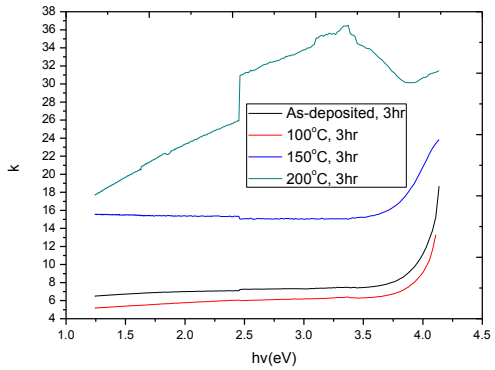

Fig. 18. Plots of k versus hv of film samples at 3 hours deposition time at different annealing temperature

The index of refraction n is an important parameter for optical applications. The complex optical refractive index is described according to the relation [34].

$$\bar{n} = n(w) + ik(w) \tag{4}$$

where n is the real part of and k is the imaginary part (extinction coefficient) of the complex refractive index. We determined the refractive index of our samples using the relation [35]. Fig 19 shows the plots of refractive index against photon energy for films deposited at 1 hour while Fig. 20 and 21 depict the refractive index versus photon energy plots for films deposited at 2 and 3 hours at different annealing temperature respectively.

$$n = \frac{1+R}{1-R} + \sqrt{\frac{4R}{(1+R^2)} - k^2} \tag{5}$$

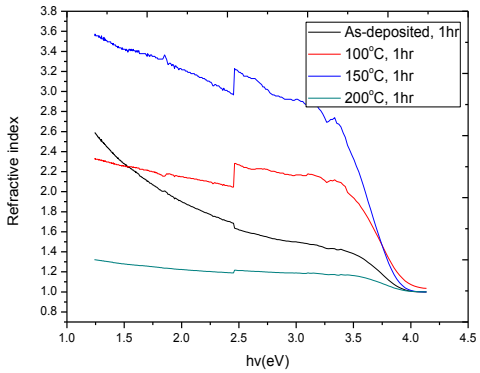

Fig. 19. Plots of n versus hv of film samples at 1 hour deposition time at different annealing temperature.

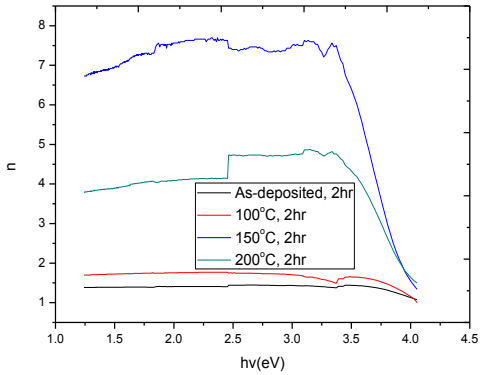

Fig. 20. Plots of n versus hv of film samples at 2 hours deposition time at different annealing temperature.

Generally, Fig. 19 to 20 indicate a rise and fall values of the refractive index with photon energy. However, a sharp decrease was observed at about 4.00eV for all film samples. The film annealed at 150°C exhibited higher refractive index values compared to other layers. A clear lack of trend with annealing temperature was observed. However, with respect to dip time, some of the film layers like the sample annealed at 200°C shows an increasing trend. This increase is due to overall increase in the reflectance with the varying parameter.

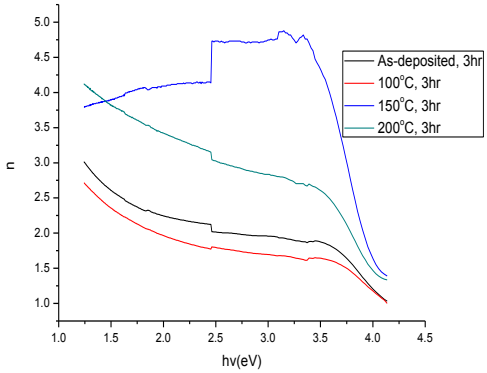

Fig. 21. Plots of n versus hv of film samples at 3 hours deposition time at different annealing temperatures.

The EDXRF analysis for CeO thin films is displayed in Fig. 22. The Figure shows that peak for cerium (Ce) was recorded at 6.4KeV. Smaller peak of Ce was also recorded at energy of 7.0KeV, while oxygen peaks were recorded at energies of 0.2KeV and 0.4KeV respectively confirming the formation CeO from EDXRF analysis. The peaks for other elements could have come from glass and some impurities.

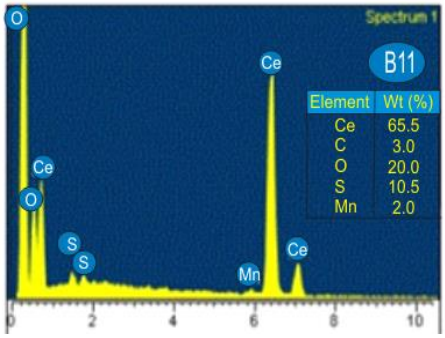

Fig. 22. EDXRF for CeO Thin Film

4. Conclusions

Chemical Bath Deposition process has been employed for deposition of cerium oxide using cerium acetate precursors with emphasis on the effect of deposition time and annealing temperature on the optical properties of the films. The optical properties investigated showed considerable variation with the deposition parameters. In particular, the band gap exhibited red shifts for some film samples and blue shifts for other film samples while some samples showed no trend with the growth parameters. In general, this research has showcased optical properties essential for potential solar cells fabrication, optoelectronic, architectural materials etc.

References

[1] D. S. Dhawale, A. M. More, S. S. Latthe, X. Y. Rajpure, C. D. Lokhande, Appl. Surf. Sci., **254**, 3269 (2008).
[2] C. Mansilla, Solid State Sciences **11**(8), 1456 (2009).
[3] G. Balakrishnan, P. Kuppusami, T. N. Sairam, R. Birumurugesan, E. Mohandas,

D. Sastikumar, Journal of Nanoscience and Nanotechnology **9**(9), 5421 (2009).
[4] D. Camino, D. Deroo, J. Salardenne, N. Treuil, Solar Energy Materials and Solar Cells **39**(2), 349 (1995).
[5] A. Al-Kahlout, D. Vieira, C. O. Avellaneda, E. R. Leite, M. A. Aegerter, A. Pawlicka, Ionics **16**(1), 13 (2010).
[6] J. Wang, B. Zhang, M. Shen, Journal of Sol-Gel Science and Technology **58**(1) 259 (2011).
[7] A. Trovarelli, Catalysis Reviews **38** (4), 439 (1996).
[8] J. F. D. Lima, R. F. Martins, C. R. Neri, O. A. Serra, Applied Surface Science **255** (22), 9006 (2009).
[9] F. E. Ghodsi, F. Z. Tepehan, G. G. Tepehan, Surface Science **601**(18), 4497 (2007).
[10] D. Channei, A. Nakaruk, S. Phanichphant, P. Koshy, C. C. Sorrell, Journal of Chemistry **2013**, 1 (2013).
[11] G. Balakrishnan, S. T. Sundari, P. Kuppusami et al., Thin Solid Films **519** (8), 2520 (2011).
[12] B. B. Patil, S. H. Pawar, Journal of Alloys and Compounds **509**(2), 414 (2011).
[13] N. Savvides, A. Morley, S. Gnanarajan, A. Katsaros, Thin Solid Films **388**(1-2), 177 (2001).
[14] H. Unuma, T. Kanehama, K. Yamamoto, K. Watanare, T. Ogata, M. Sugawara, Journal of Materials Science **38**, 255 (2003).
[15] S. D. Sartale, C. D. Lokhande, Ceramics International **28**(5), 467 (2002).
[16] Lambert-Beer's law Source: http://www.wikilectures.eu/index-php?oldid-24362.
[17] C. Augustine, M. N. Nnabuchi, Journal of Ovonic Research **13**(4), 233 (2017).
[18] C. Augustine, M. N. Nnabuchi, Journal of Non-Oxide Glasses **9**(3), 85 (2017).
[19] C. Augustine, M. N. Nnabuchi, F. N. C. Anyaegbunam, A. N. Nwachukwu, Digest Journal of Nanomaterials and Biostructures **12**(2), 523 (2017).
[20] C. Augustine, M. N. Nnabuchi, Optical and solid state properties of chemically deposited CuO/PbS double layer thin film, Materials Research Express, http://doi.org/10.1088/2053-1591/aaf11 (2018).
[21] M. N. Nnabuchi, C. Augustine, Mn_3O_4/PbS thin film: Preparation and effect of annealing temperature on some selected properties, Materials Research Express, https://doi.org/10.1088/2053-1591/aab589 (2018).
[22] S. Srikanth, N. Suriyanarayanan, S. Prabahar, V. Balasubramanian, D. Kathirvel, Advances in Science and Research **2**, 95 (2011).
[23] B. Ismail, S. Mushtaq, A. Khan, Chalcogenide Letters **11**(1), 37 (2014).
[24] M. N. Nnabuchi, Pacific Journal of Science and Technology **7**(1), 69 (2006).
[25] M. N. Nnabuchi, Pacific Journal of Science and Technology **6**(2), 105 (2005).
[26] I. Kaur, D.K. Pandya, K.I. Chopra, Journal of Electrochemical Society, **127,** 943-948 (1980).
[27] K.L. Chopra, P.D. Paulson, V. Dutta, Prog Photovolt:Research Applications, **12**, 69-92 (2004).
[28] C. D. Lokhande, B. R. Sankapal, S. Mane, H. M. Pathan, M. Muller, M. Giersig, V. Ganesan, Appl. Surf. Sci. **193**, 1 (2002).
[29] V. Bilgin, S. Kose, F. Atay, I. Akyuz, Mater. Chem. Phys. **94**,103 (2005).
[30] Y. Natsume, H. Sakata, T. Hirayama, Phys Stat Sol (A) **148**, 485 (1995)
[31] S. J. Ikhmayies, R. N. Ahmad-Bitar, Journal of Materials Research and Technology **2**(3), 221 (2013).
[32] A. Igweoko, C. Augustine, N. E. Idenyi, B. A. Okorie, F. N. C. Anyaegbunam, Materials Research Express (2018).
[33] B. G. Mahrov, A. Hgfeldt, L. Dloczuk, T. Dittrich, Appl. Phys. Lett. **84**(26), 5455 (2004).
[34] K. Kamiya, J. Cookson, Plantinum Metals Rev. **56**, 83 (2014).
[35] J. S. Cruz, D. S. Cruz, M. C. Arenas-Arrocena, F. D. M. Flores, S. A. M. Hernandez, Chalcogenide Letters **12** (5), 277 (2015).